
Article:
Williamson, S., Griffo, A., Stark, B. et al. (2016) A controller for single-phase parallel inverters in a variable-head pico-hydropower off-grid network. Sustainable Energy, Grids and Networks, 5. pp. 114-124. ISSN: 2352-4677

https://doi.org/10.1016/j.segan.2015.11.006

A Controller for Single-Phase Parallel Inverters in a Variable-Head Pico-Hydropower Off-Grid Network

S. J. Williamson [a]*, A. Griffo [b], B. H. Stark [a], J. D. Booker [a]

[a] Faculty of Engineering, University of Bristol, Bristol, BS8 1TR, UK

[b] Department of Electrical & Electronic Engineering, University of Sheffield, Sheffield, S1 3JD, UK

* Corresponding Author: Tel: +44 117 331 5464, Email: sam.williamson@bristol.ac.uk

Abstract

The majority of off-grid pico-hydropower systems use a single turbine and generator, connected directly to an AC network resulting in clusters of isolated, power-limited, single failure-prone networks. The use of inverters has been previously proposed in order to decouple the turbine's rotational speed from the network frequency in these remote microgrids. This facilitates the use of multiple generators and the creation of expandable, reliable networks with redundancy. This paper presents an inverter controller for this situation, and addresses a combination of challenges that is specific to expandable pico-hydropower networks in geographically dispersed remote communities. Multiple variable-head turbines are connected to a network, whose individual local hydraulic heads vary due to flow changes over the seasons, and the network has no single generator that dominates and no master controller, but instead identical independent controllers that do not communicate. The controller presented here uses an output voltage and frequency droop controller, with inner synchronous reference frame control loops for the fundamental voltage and current. The control coefficients are automatically adjusted to the available local hydraulic head. Simulation and experimental results show that the power is shared amongst generators, proportionally to the locally available power, in steady and dynamic situations. Harmonic compensation loops are proposed: these reduce the output total harmonic distortion (THD) of a single inverter from 9.53% to 1.45% for a non-linear load. Geographically distributed operation in resistive networks is investigated, and the results show that the controller achieves plug-and-play capability for remote off-grid networks with multiple and different pico-hydropower generators.

Keywords – Parallel inverter control, Pico hydropower, Single-phase, Droop control, Rural electrification.

1. INTRODUCTION

Pico hydropower has been used for many decades as a method of delivering rural electrification. It has been shown to be a cost effective method of off-grid electricity generation, especially in hilly and mountainous regions [1]. A standard pico-hydro system is a stand-alone unit, comprising a turbine driving a generator, a shunt controller, known as an electronic load controller (ELC) regulating either the voltage or frequency output, and a low-voltage distribution system with consumer loads, such as lighting, mobile phone chargers and radios [2, 3]. The turbine is designed to operate at a constant speed to generate the grid frequency; the ELC maintaining a constant load on generator. Fluctuations in the environmental conditions, such as a drop in flow rate or head, can cause the system to shut down. Over time, consumer demand on the system increases as they purchase more electrical equipment, up to the point where the increased demand causes severe voltage drop in peak load times and often the circuit breaker at the generator to trip. Therefore, there is a demand for methods to connect multiple hydropower generators and expand the off-grid network as more capital becomes available. A straightforward method is to connect micro-hydro units through synchronizer units directly to the grid. This is implemented in a recent 11 kV off-grid network containing six micro-hydro units, constructed in Western Nepal by the Alternative Energy Promotion Centre [4]. Due to the direct connection of induction generators, power quality and sharing are not controlled, and changes in head strongly affect power sharing, risking a loss of synchronization. A potential solution is to use a power electronic interface per turbine. For example, a rectifier is followed by a DC-DC converter that feeds the DC link of a single-phase inverter. This allows the turbine to operate at its optimal head- and flow-dependent frequency, with grid voltage and power flow regulation performed using techniques similar to those reported for grid-connected and off-grid microgrids. An example system implementation in a rural off-grid network is shown in Fig. 1 (a), with the schematic system diagram shown in Fig. 1 (b).

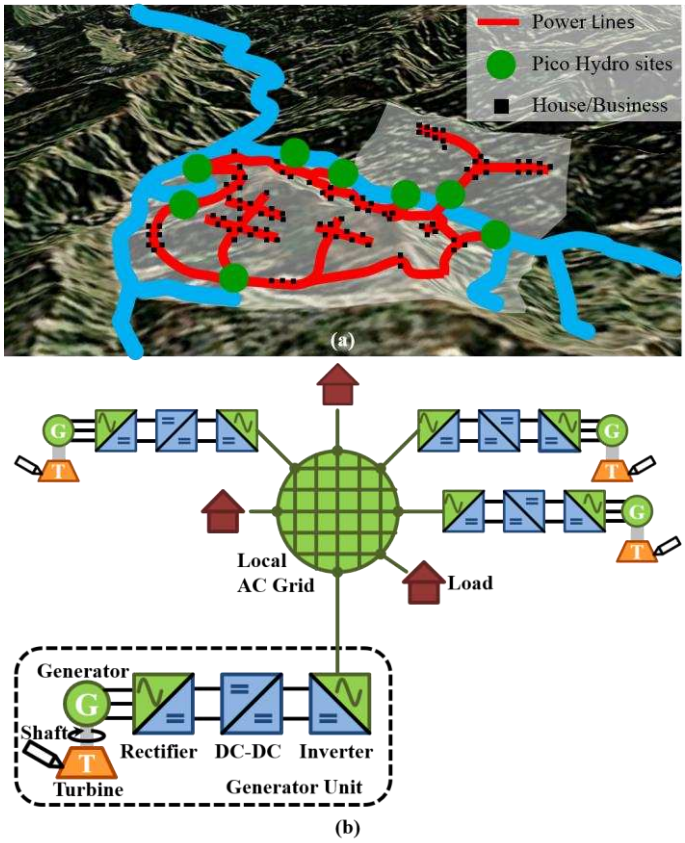

Fig 1. (a) Example variable head pico hydropower off-grid network implementation. (b) Schematic diagram of the off-grid network and energy conversion system.

This paper proposes the controller for the single-phase inverter interface. The main aim is to enable a pico-hydro network with an arbitrary number of turbines, each with an identical controller with no master controller or communication between controllers. The main differentiators to the literature are that the controller adapts to seasonally and spatially varying hydraulic conditions, and it does not require the network to be grid-connected or have a generator that dominates supply. This controller provides an essential component for a pico-hydro network that can be interconnected and expanded to increase capacity and redundancy.

Parallel inverter control has 5 basic requirements [5]: voltage and frequency regulation; power sharing between units; output power quality; synchronization; and fault and islanding protection. The first 4 requirements are examined in this paper. Controlling parallel inverter interfaces without communication requires the closed-loop regulation of voltage and frequency using local measurement of voltage and current. This is normally achieved through droop control [6-12], emulating the response of a synchronous

generator connected to a grid. There are alternative methods proposed in the literature, such as augmenting the control with an average power control technique [13] or controlling the inverter to behave as a synchronous machine [14, 15]. A secondary control loop can also be used to restore the network voltage or frequency to its nominal levels [16].

Utilizing droop control requires a trade-off between the voltage and frequency regulation and the power sharing capability of the system [7]. In the approach reported on here, loose regulation is required to achieve power sharing between geographically-dispersed generators on a low-voltage (resistive) network. Power sharing between units with different input power can be improved by adjusting the droop coefficients [8] and virtual impedance [9] with the input power. The output power quality can be controlled using a single virtual impedance [16] or set of band-pass filters in the virtual output impedance [7] or through a series of harmonic droop controllers [17]. Synchronization between parallel inverters has been achieved through using a large variable physical [10] or virtual [7] impedance or a phase-locked-loop [18]. There are many examples in the literature of parallel inverter control schemes, such as those in the references above, but none that have been interfaced with a variable-input-power pico-hydro system.

The paper is structured as follows: Section 2 develops the control system, derives the inner current, voltage and harmonic controller transfer functions, and shows respective bode plots. The section also addresses: automated adjustment of droop coefficients and virtual output impedance as a function of the available turbine power; power sharing proportional to each unit's available power; plug-and-play capabilities enabling interconnection of additional units, each capable of working in load sharing or grid forming mode; and compensation of harmonic distortion caused by nonlinear loads. Section 3 demonstrates the controller performance by simulation. Section 4 describes the experimental test facility, and finally Section 5 presents scale experimental results for voltage quality and power sharing ratios with unequal transmission line length and source power.

2. CONTROL SYSTEM DESIGN

The design of the control system is discussed in the following Section, with the 4 functions of the parallel inverter controller discussed in detail. An overview of the control system is shown in Fig. 2.

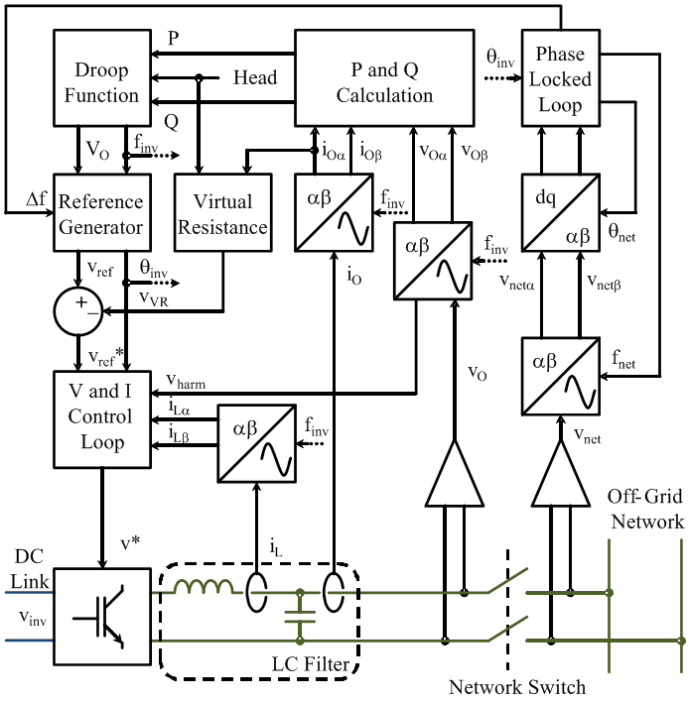

Fig. 2. Control System Structure

2.1. Voltage and Frequency Regulation via Droop Control

Droop control adjusts the output voltage and frequency of an inverter in order to establish a desired relationship between supplied active and reactive power and measured local voltage and frequency. The relationships depend on the line and inverter output impedances [10]. Typically, transmission lines are considered to be inductive, e.g. in [6], however the network considered here operates at low voltage (240 V_{RMS}) therefore resistive lines are assumed and the droop equations are [7]

$$f = f_0 + mQ \qquad (1)$$

$$V_O = V_{O,0} - nP \qquad (2)$$

where f is the output frequency, f_0 is the output frequency set point, m is the reactive power droop coefficient, Q is the measured reactive output power, V_O is the output voltage reference, $V_{O,0}$ is the output voltage set point, n is the active power droop coefficient and P is the measured active power. Although this

relationship is designed for a low-voltage, resistive-line network to be used with identical controllers, it has been shown to also operate in conjunction with inductive- or capacitive-line based droop control [20].

The droop coefficient is in the forward path of the controller, therefore the transient response of the control is dependent on droop coefficients, m and n [7]. Ideally, these should be large to have good transient response and also allows for accurate power sharing, but this would cause a large variation in the regulated voltage and frequency. The regulation is also typically defined in the system specification, fixing the droop coefficients. Therefore, to improve the transient response of the control system, additional terms can be included. In this system a differential term is included in the droop equations, as described in [7], as integral terms can cause instabilities with resistive line droop equations. Therefore (1) and (2) become

$$f = f_0 + mQ + m_d \frac{dQ}{dt} \quad (3)$$

$$V_O = V_{O,0} - nP - n_d \frac{dP}{dt} \quad (4)$$

where m_d and n_d are the differential constants. The reference voltage waveform is then constructed from these values of output voltage and frequency.

The impedance of the transmission lines in off-grid networks and the inverter output impedance are neither purely inductive nor resistive which leads to cross-coupling in the droop function [10]. A virtual output impedance can be used to force these to seem either inductive or resistive, dependent on the control scheme selected, and allow the droop function to be completely decoupled [7]. In this scheme, as resistive lines are assumed, this is achieved by multiplying the fundamental component of the measured output current i_O by a virtual resistance gain R_V and then subtracting this from the reference voltage calculated by the droop function.

2.2. Power Sharing

Standard droop control, utilizing steep droop coefficients, is able to share power well with units that have equal rated power. However, when there are unequally rated units on the system, then the power sharing is not proportional to the rated output of the system, so smaller units will have a larger proportion of their output supplied to the system. The droop coefficients and virtual resistance can be made dependent upon

the input power, which assists in achieving accurate power sharing proportional to the unit's available input power [8, 9], which have been used for UPS inverters. In the presented case, the input power is dependent on the head at the turbine. Therefore, a model for the turbine can be used to determine the maximum power available at the turbine for a given head, $P_{(TURB,MAX)\,(H)}$., such as those found in [20-23]. Alternatively, if there is experimental data for the turbine performance across its head range, a look-up table of the maximum available turbine power can be included for each measured head. For this paper, a low-head Turgo turbine model theoretically derived and experimentally validated in [20] is used, and therefore the maximum currently available turbine power can be calculated for the measured turbine head. The available power characteristic as a function of the available head and turbine rotational speed used is shown in Fig. 3.

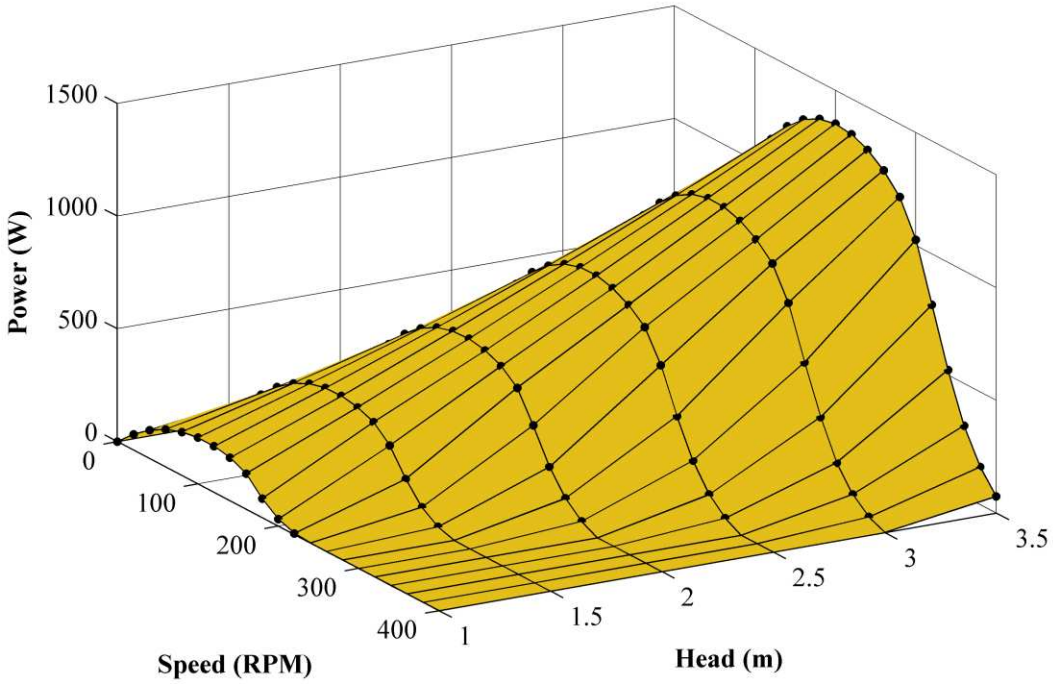

Fig. 3. Theoretical power model for turbine for head ranging from 1.0 to 3.5 m [20].

From this, a normalized turbine power output, the ratio of $P_{TURB,MAX}(H)$ to the maximum possible turbine output power $P_{TURB,MAX}$, a fixed value, can be written as

$$\gamma = P_{TURB,MAX}(H)/P_{TURB,MAX} \quad (5)$$

Then the droop coefficients and virtual resistance are set to

$$m = m_{MAX}/\gamma \quad (6)$$

$$n = n_{MAX}/\gamma \quad (7)$$

$$R_V = R_{V,MAX}/\gamma \qquad (8)$$

where m_{MAX} and n_{MAX} are defined from the regulated range of frequency and output voltage and the maximum output active and reactive powers and $R_{V,MAX}$ is the maximum power virtual resistance. In this way, as γ reduces the gradients of the droop curves become steeper. So in the case of the P vs. V_O droop curve, for the same output voltage, the active power delivered is reduced.

The stability of the system resulting from the interconnection of multiple generation units with dynamically changing heads is potentially challenging, with short term system stability and longer term power system stability. In this paper, we assume that the flow rate is nearly constant, with changes happening over a significantly longer time-scale than the proposed controller, e.g. days vs. tens of milliseconds. Under this reasonable assumption the instantaneous output power control and the load management can be assumed to be decoupled. Load management issues can then potentially be guaranteed with an appropriate supply/demand management strategy.

2.3. Power Measurement

The droop function, (3) and (4), needs the line-cycle-averaged active and reactive powers to calculate the output voltage and frequency. In 3-phase systems this can be achieved by using the Clarke transform to convert the line values into orthogonal α and β components. The instantaneous powers are calculated using

$$P = \left(v_{O\alpha} i_{O\alpha} + v_{O\beta} i_{O\beta}\right)/2 \qquad (9)$$

$$Q = \left(v_{O\beta} i_{O\alpha} - v_{O\alpha} i_{O\beta}\right)/2 \qquad (10)$$

which are used as inputs for the droop function. For single-phase systems, there are several different methods to achieve the conversion between a single-phase sinusoidal signal and αβ components, such as shifting the signal by 90° using a transport delay [7], integrating the incoming signal [24] or using a resonant filter [25], which is based on a Second Order Generalised Integrator (SOGI) [18]. A modified version of this SOGI-based filter is proposed in [26], where an additional gain is included in the orthogonal (β) path, and the gains are calculated using a Kalman function. An alternative method using a Reduced Order Generalised Integrator (ROGI) based filter has been proposed in [27], where the filter is implemented in the synchronous reference frame which reduces the number of states in the implementation,

allowing for a reduced computational overhead, however this can only be implemented for 3-phase systems as it requires the stationary reference frame components as an input. The method used in this paper has an identical structure to that presented in [26], but with constant gain values calculated using the method in [26]. The resonant frequency used in the filter is calculated from the droop function, (3), and is fed into the filter, allowing the filter to adapt to any variation in the grid frequency. The structure of the SOGI-based filter is shown in Fig. 4 (a).

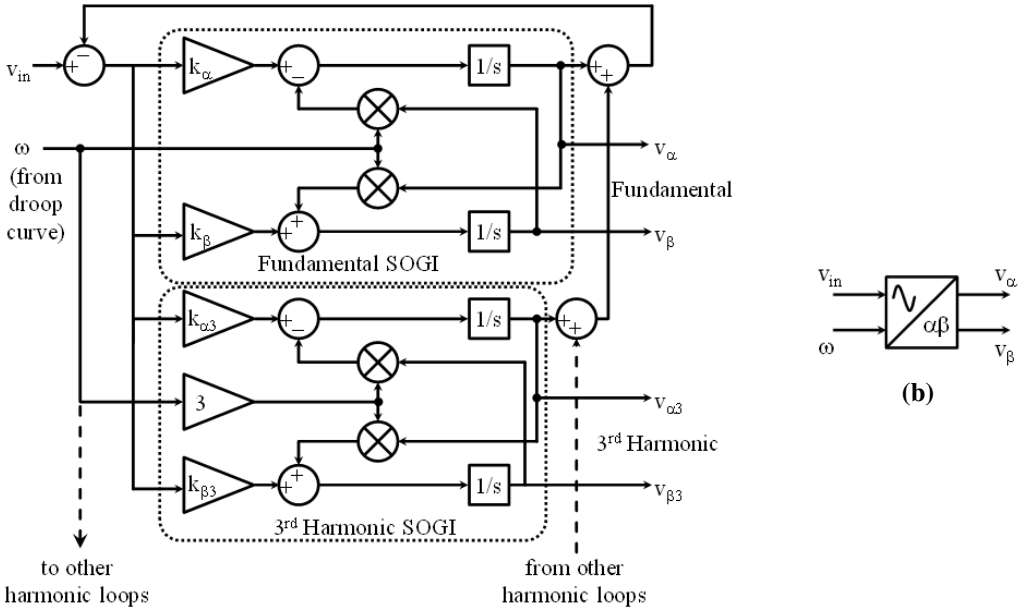

Fig. 4. (a) Second Order Generalised Integrator (SOGI) based filter with additional harmonic loops. (b) Symbolic representation of SOGI-based filter.

Additional resonant loops can be added to filter any harmonics in the input [28], as shown in Fig. 4 (a) where a 3rd harmonic loop is included. The harmonics from each additional loop can be extracted and used if needed. Fig. 4 (b) shows the symbol used for the SOGI-based filter in the following Sections.

2.4. Fundamental Voltage Controller

A second order LC filter is assumed at the output of the inverter. Similar to the control structure commonly employed in three-phase grid connected inverters and active rectifiers [29, 30], a synchronous reference frame controller is employed here for both the outer output capacitor voltage and inner inductor current control loops. A similar approach has been used in [11] where the outer voltage loop is transformed into the synchronous frame, before being returned into the stationary frame for the current control loop.

This current loop is a proportional loop with a feed-forward term, which reduces the need for a large gain to reduce the steady-state error. Similar control strategies are proposed in [31-33], where the systems described are either already in three-phase or use delays to create the orthogonal component.

Here, the control scheme shown in Fig. 5 is employed to control the inverter output voltage. This is different to [11] as it uses the synchronous reference frame throughout the control of voltage and current, allowing simple PI control to be used in both and ensuring a zero steady state error. Reference [31] uses the synchronous reference frame throughout the controller, but the presented controller differs as the reference voltage generated from the droop function and measured voltage and currents are transformed into the dq synchronous reference frame using the SOGI-based filter. The αβ to dq transform, and inverse, is synchronized with the angle fed forward from the droop equations, (3), not through a PLL loop as normally used. PI loops are then used to force the measured d-axis voltage to its reference and the q-axis voltage to zero.

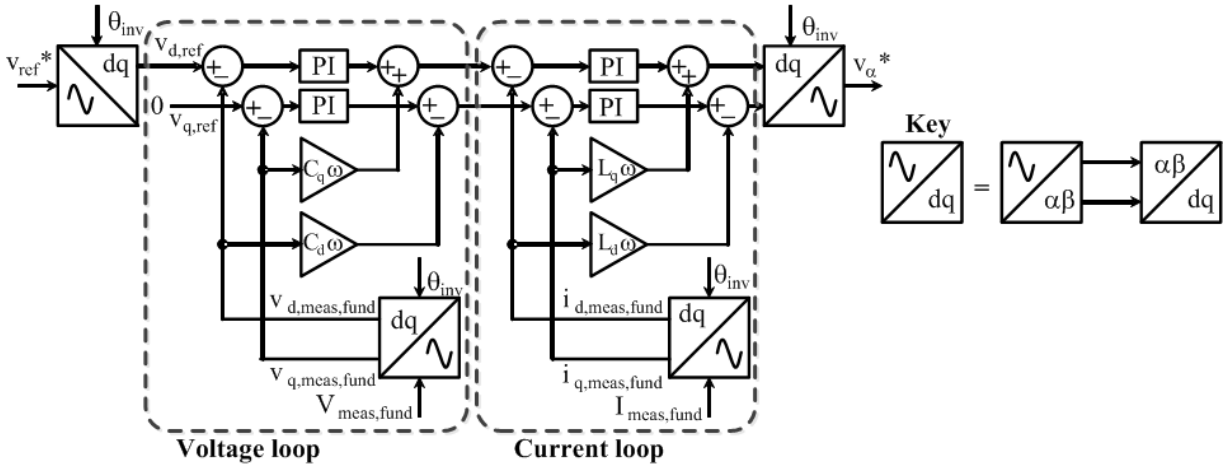

Fig. 5. Proposed voltage and current controller using synchronous reference frame.

To derive a transfer function for the inner current loop and outer voltage loop, the control loops first need to be simplified. The actual voltage and current control loop in the synchronous frame, based on Fig. 5, is shown in Fig. 6 (a). It is assumed that the cross-coupling between the d and q axes due to the reference frame transformation is compensated in the controller design, using the feedforward terms $\pm\omega_{inv}Cv_{d,q}$ and $\pm\omega_{inv}Li_{d,q}$ [28]. Therefore, cross-coupling is omitted from voltage and current controller analysis based on the block diagram in Fig. 6 (a) which can be further simplified to the block diagram in Fig. 6 (b) using

simple manipulations. In these manipulations, the SOGI-based filter in the voltage loop is moved from the feedback and input path into the system to allow for this simplification.

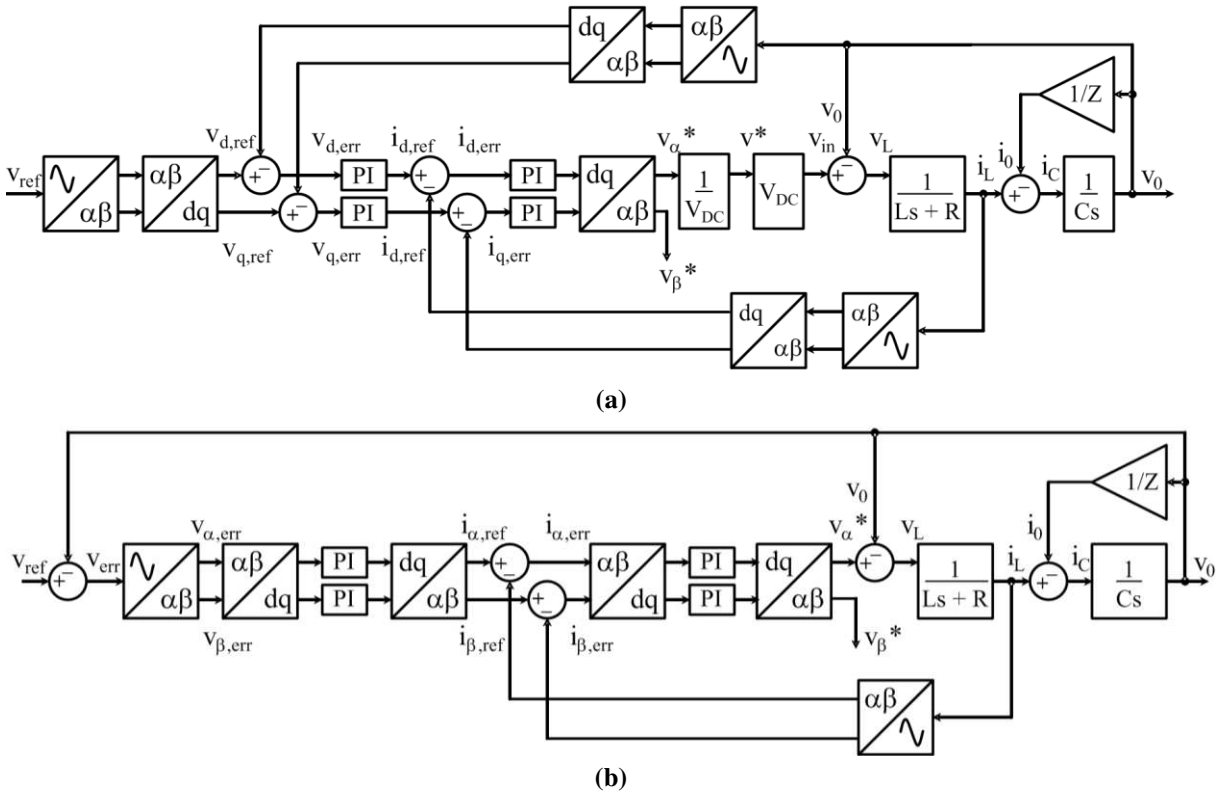

Fig. 6. (a) Actual and (b) simplified voltage and current control loops.

It has been shown that a PI controller in the synchronous reference frame is identical to a Proportional + Resonant (P+R) controller in the stationary reference frame [11] [34]. This is exploited in the derivation of the control loop transfer function, where the block diagram shown in Fig. 7 is equivalent to

$$\begin{bmatrix} v_\alpha^* \\ v_\beta^* \end{bmatrix} = \begin{bmatrix} k_p + \dfrac{k_i s}{s^2+\omega^2} & -\dfrac{k_i \omega}{s^2+\omega^2} \\ \dfrac{k_i \omega}{s^2+\omega^2} & k_p + \dfrac{k_i s}{s^2+\omega^2} \end{bmatrix} \begin{bmatrix} i_{\alpha,err} \\ i_{\beta,err} \end{bmatrix} \qquad (13)$$

where k_p and k_i are the proportional and integral gains of the controller, and ω is the signal frequency.

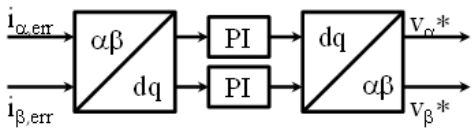

Fig. 7. Synchronous reference frame PI controller, mathematically equivalent to a P+R controller

From the block diagram in Fig. 6 (b) and using (13), the transfer functions of the inner current loop and outer voltage loop are derived. The inner current loop transfer functions are

$$i_L = G_4 i_{\alpha,ref} + G_5 i_{\beta,ref} \qquad (14)$$

where G_4, G_5 are listed in the Appendix. The Bode plots in Fig. 8 show the frequency response for the inner current loop for the transfer functions in (14), $i_L/i_{\alpha,ref}$ and $i_L/i_{\beta,ref}$, when L = 3 mH, C = 30 μF, R_L = 0.1 Ω, Z_{LD} = 100 Ω, and PI controller gains set to k_{pi} = 2, k_{ii} = 10, k_{pv} = 0.1 and k_{iv} = 1.

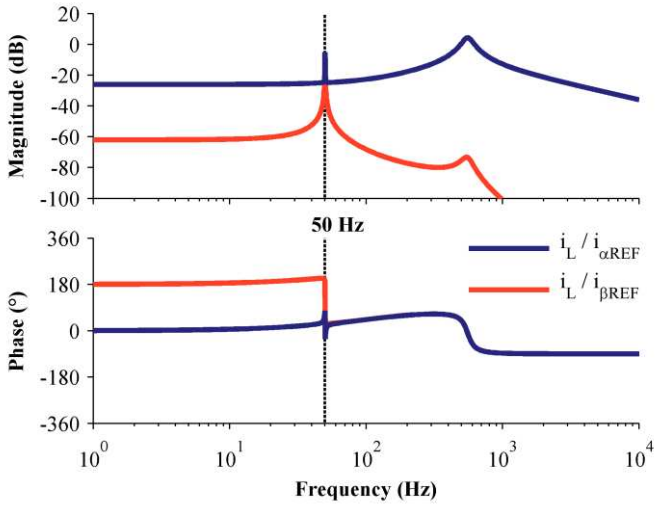

Fig. 8. Inner current loop Bode plots.

As can be seen in Fig. 8, the inner current controller has a resonant peak at 50 Hz, the line frequency, which is expected as the SOGI-based filter rejects all harmonic components and the PI controller in the dq reference frame acts as a resonant controller in the stationary frame, with the resonant frequency at the line frequency.

Similarly, the outer voltage loop transfer function is

$$v_O = \frac{G_6(G_4G_7 + G_5G_8)}{1 + G_6(G_4G_7 + G_5G_8)} v_{ref} \qquad (15)$$

where G_{4-8} are defined in the Appendix. The frequency response of the transfer function in (15) is shown in Fig. 9, with PI controller gains k_{pv} = 0.1 and k_{pi} = 1, and the other variables as for the current loop.

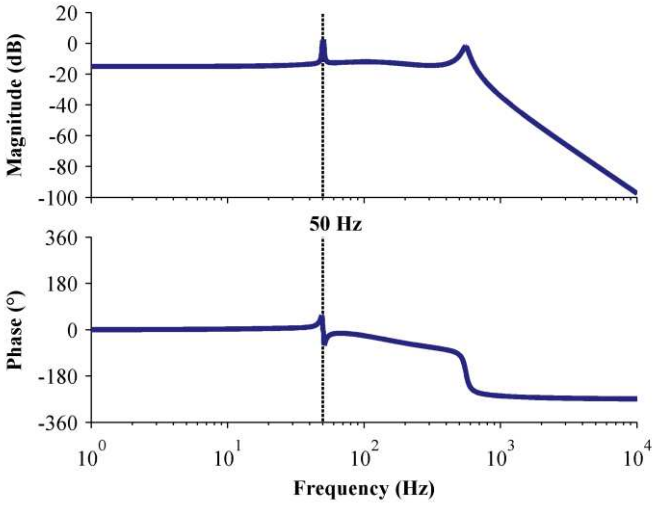

Fig. 9. Fundamental voltage controller Bode plot.

Again, the voltage loop shows a resonance at the line frequency of 50 Hz. Both of these controllers, in Figs. 8 and 9, exhibit the proportional plus resonant qualities of operating at a single line frequency in the controller, whilst being able to control the system with a proportional-integral controller, with the zero steady-state error benefits that this design brings. The resonance at 530 Hz in Figs. 8 and 9 is due to the LC filter.

The choice of the controller gains involves several trade-offs: As discussed in [11], the proportional gain is responsible for the transient response of the controller, whilst the steady state performance at the resonant frequency is dependent on integral gain. This is demonstrated in Fig. 10 below, where the proportional and integral constants for the voltage controller are perturbed by a factor of 10 in each direction to show the effect on the frequency response. As can be seen in Fig. 10 (a), as the proportional gain decreases, the filtering of the low and high frequency noise is improved. Reducing the gain too far, however, slows the transient response of the controller as the gain is in the forward path of the loop. Fig. 10 (b) shows that as the integral gain increases, the bandwidth of the resonant part of the controller increases. This would cause additional low frequency noise to be passed through the controller. However, the integral gain needs to be chosen to be high enough to ensure that there is a large steady state gain around the fundamental frequency to allow for any small variations in the grid frequency.

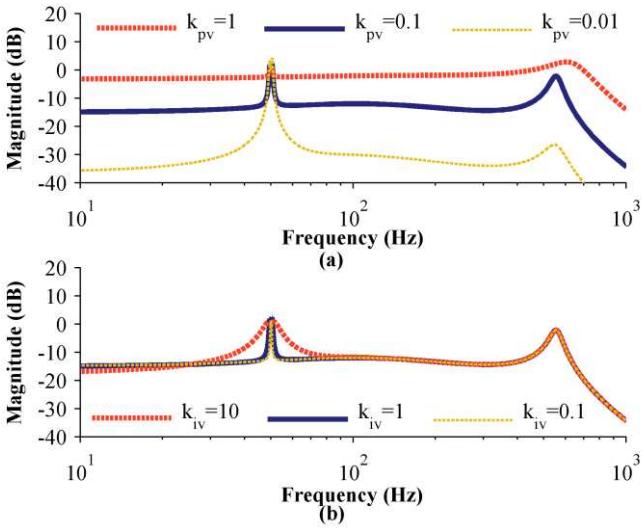

Fig. 10. Bode plots for the voltage controller, v_O / v_{ref}, for perturbed (a) proportional and (b) integral gains.

2.5. Harmonic Voltage Controller

In single-phase applications, harmonic distortion compensation has been recently proposed in [12] where band-pass virtual resistances are employed at the point of common coupling, providing a power filter prior to the load. In three-phase grid connected inverters and active power filters applications, harmonic compensation using a series of synchronous frame harmonic voltage PI controllers, or Proportional-Resonant controllers have been proposed in [29, 30, 35, 36]. Similar to the three-phase strategies, here the output voltage harmonics are suppressed using a series of synchronous frame harmonic voltage PI controllers at the inverter output, as with the fundamental voltage controller described above. As shown in Fig. 11, the measured harmonic output voltages, extracted from the SOGI-based filters in Fig. 2, are transformed into the dq reference frame. Using a PI controller, the measured harmonic voltages are forced to zero. These are transformed back into the αβ reference frame, and the α component becomes the reference waveform from the harmonic. All the harmonic reference waveforms are summed to form the final reference, which is output to the PWM generator.

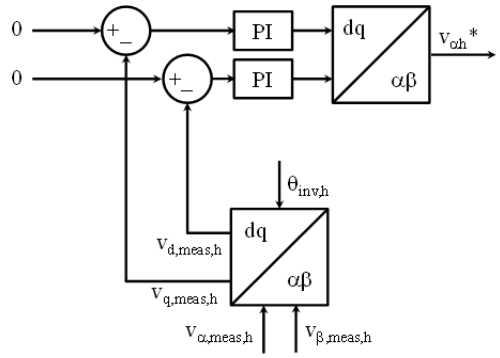

Fig. 11. Harmonic voltage controller in synchronous reference frame

As with the fundamental voltage controller, the harmonic voltage control loop, shown in Fig. 12 (a), is equivalent to Fig. 12 (b) which allows the derivation of the transfer function. For normal operation, $v_{ref,h}$ is set to zero.

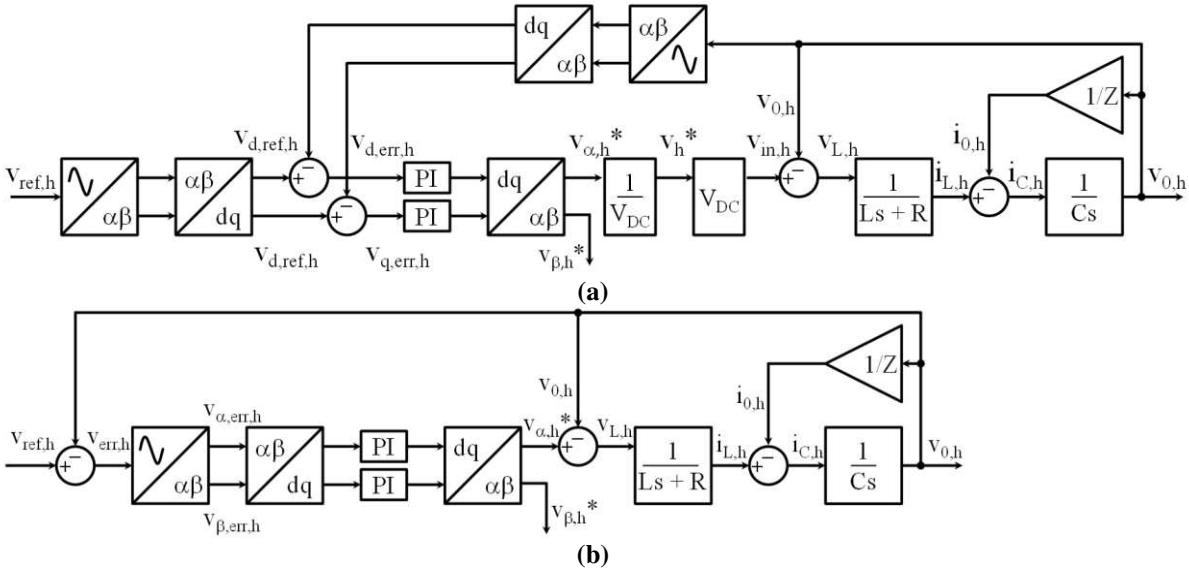

Fig. 12. (a) Actual and (b) simplified harmonic voltage control loop

Using the same techniques as the fundamental voltage controller, the transfer function for the h^{th} harmonic is derived. The transfer function is

$$v_{0,h} = \frac{\left(G_{3,h}\left(G_{1v,h}G_{\alpha,h} - G_{2v,h}G_{\beta,h}\right)\right)}{1 + \left(G_{3,h}\left(G_{1v,h}G_{\alpha,h} - G_{2v,h}G_{\beta,h}\right)\right)} v_{ref,h} \qquad (16)$$

where all matrices are defined in the Appendix. The Bode plot for this transfer function at the 3rd, 5th and 7th harmonic frequencies, along with the fundamental voltage control loop, is shown in Fig. 13, with PI gains $k_{pvh} = 0.1$ and $k_{ivh} = 1$ for the third and 5th harmonics and $k_{pv7} = 0.1$ and $k_{iv7} = 2$, and all other parameters as in the voltage and current loop.

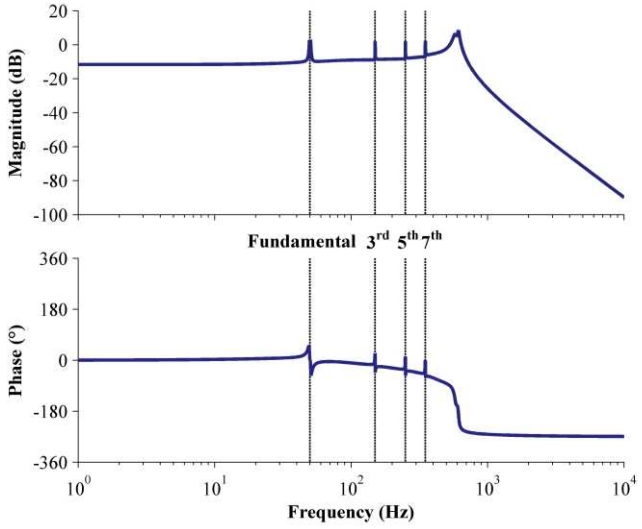

Fig. 13. Bode plots for voltage harmonic controller at 3rd, 5th and 7th harmonics, including the fundamental voltage loop

Fig. 13 shows the harmonic resonant peaks at each of the harmonic frequencies, 3rd, 5th and 7th as well as the fundamental loop. The complete voltage loop acts as a band-pass filter, allowing the selected harmonics through the controller and then can force them to zero through the PI control. Additional loops for higher order harmonics can be easily added, but at the cost of a larger computational overhead, up to the limit of implementing the controller in the discrete time domain.

2.6. Phase Locked Loop (PLL)

The standard way of synchronization is for the network voltage to be transformed into the synchronous reference frame via the αβ stationary reference frame, with the network angle found by forcing the q-axis component to zero. Advanced PLL strategies are presented in [18, 37-41], using a synchronous reference frame or digital non-linear methods. Here, a synchronous reference frame based PLL is used, with a single-phase input. The transformation of the voltage signal from a single-phase signal to the αβ reference frame can be achieved using the SOGI-based filter again, as in [18] and analysed in [37], and shown in Fig. 14.

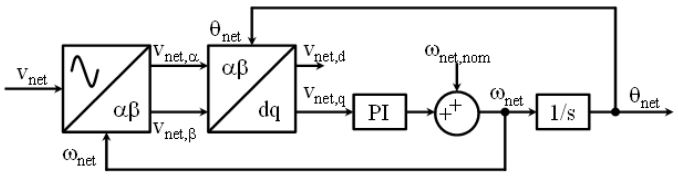

Fig. 14. SOGI-based phase-locked loop.

The off-grid network angle θ_{net} is then compared with the inverter angle θ_{inv}. This error is passed through a proportional controller and fed back into the droop function to change the frequency of the inverter to

match the grid frequency. Once the error is below the critical value ε_{crit}, the switch between the inverter and the grid is closed with a latch to ensure that there is no chattering.

3. SIMULATION

Using the control system described in Section 2, a simulation is constructed to validate the controller design and investigate the system responses to different loads and arrangements. Each inverter is connected through a switch, controlled by the PLL, onto an AC bus-bar representing the off-grid network with linear and non-linear loads. The simulation and following experimental work take place at low voltage, to prove the control concept. The simulation parameters used in the controller are shown in Table 1.

Table 1. Converter parameters used in simulations and experiments

Parameter	Value	Parameter	Value	Parameter	Value
V_{inv}	400 V	m_{MAX}	0.0046 Var/Hz	k_{pvd5}, k_{pvq5}	0.1
f_0	50 Hz	n_{MAX}	0.022 W/V_{RMS}	k_{ivd5}, k_{ivq5}	1
$V_{O,0}$	250 V_{RMS}	m_d	0.00005 Hz/Var s	k_{pvd7}, k_{pvq7}	0.1
L	3 mH	n_d	0.00005 V/W s	k_{ivd7}, k_{ivq7}	2
C	30 µF	k_{pvd}, k_{pvq}	0.1	k_{pid}, k_{piq}	3
$R_{V,MAX}$	4 Ω	k_{ivd}, k_{ivq}	1	k_{iid}, k_{iiq}	15
f_{sample}	7 kHz	k_{pvd3}, k_{pvq3}	0.1		
f_{SW}	20 kHz	k_{ivd3}, k_{ivq3}	1		

3.1. Single Inverter Operation

The droop operation of the inverter control system is demonstrated in the following simulation. Here, a single inverter is connected to 500 W load, after five seconds the load is doubled to 1000 W. The output voltage and current is shown in Fig 15.

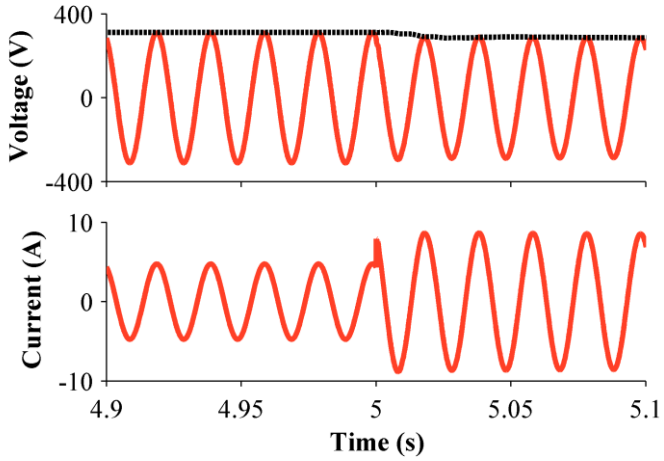

Fig. 15. Simulation of voltage drooping as current demand increases as load is doubled after five seconds

This figure shows the voltage drooping as the current doubles, as is expected in the system.

3.2. Parallel Inverter Operation

As part of their 'plug-and-play' capability, the inverters must be able to form the off-grid network and connect onto an already formed network without any manual intervention or change in control. Therefore, to test this, two inverters are connected in parallel. The first inverter is used to form the network. After five seconds a 500 W linear load is connected, and the first inverter feeds this. After a further five seconds, the second inverter is activated and connected to the network. The voltage and current traces are shown in Fig. 16 below.

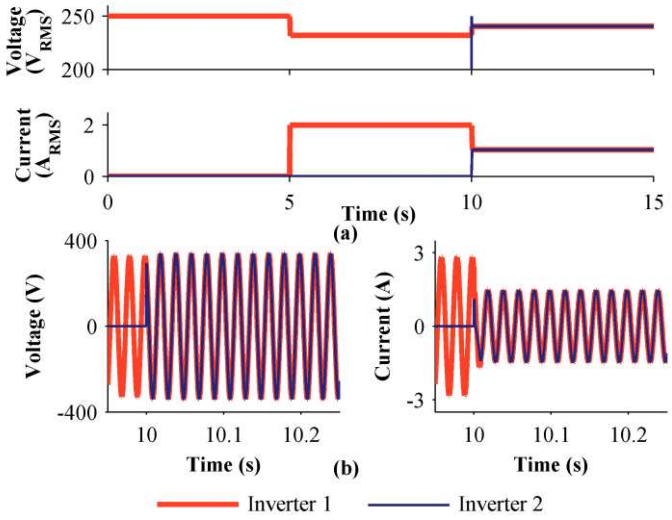

Fig. 16. Simulation of Inverter 1 forming off-grid network and inverter 2 joining at t = 10 s. (a) Voltage and current RMS values as network is formed, 500 W load is connected and second inverter is connected to network. (b) Detailed voltage and current waveforms when second inverter is connected

Fig. 16 shows the first inverter forming the off-grid network, without any load on the system. When the load is connected, the inverter output voltage droops as the load is fed. When the second inverter is connected, it synchronizes with the network through the PLL, and then connects when in phase, increasing the output voltage on the first inverters as the output active power on for this inverter is decreased.

So far it has been assumed that the inverters are equidistant from the load, however for a practical arrangement in the pico-hydro off-grid network, this is not likely to be the case, as sites will be dispersed across the landscape. Fig. 17 shows the output voltage and current waveforms for identical inverters feeding a 500 W load when $Z_{LINE1} = Z_{LINE2}$ and $Z_{LINE1} = 2 \times Z_{LINE2}$.

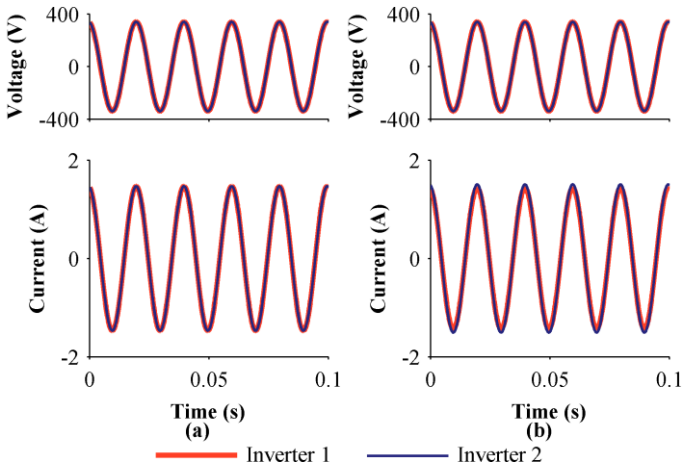

Fig. 17. Comparison between load sharing (a) with equal lines and (b) with $Z_{LINE1} = 2 \times Z_{LINE2}$

As can be seen in Fig. 17, perfect power sharing is achieved for identical line impedances, but when $Z_{LINE1} = 2 \times Z_{LINE2}$ the power sharing ratio decreases to 0.9:1.

4. Experimental Facility

Two voltage source inverters are constructed for experimentation to validate the proposed electrical arrangement and control. For safety considerations and control demonstration purposes, a low voltage prototype is considered. The inverter DC link is set at 30 V, with the output voltage set-point at 10 V_{RMS}. An 8% change is allowed in both the voltage and frequency, meaning V_O varies between 9.2 and 10 V_{RMS}. The frequency set point f_0 is 50 Hz, as this is the centre frequency of the range varying between 48 and 52 Hz.

The H-bridge inverter is constructed from four IRG4PC40UD IGBTs with bipolar PWM, driven by an in-house gate drive, with an LC filter on the output. For a 1kW version of the inverter, the inverter side DC link capacitor would be required to be 30 μF using film capacitors, which allows for a 1% voltage ripple on the DC link [42]. The output filter will have an inductance of 3 mH in a common mode arrangement, with a capacitance of 30 μF, the output filter therefore provides a corner frequency of 530 Hz.

The switching frequency is 20 kHz. The transmission lines are represented by resistors, which connect the inverter with a bus bar. The loads, either a linear resistive load or a non-linear load comprising a diode bridge rectifier, capacitor and resistor, are connected on to the bus bars via another pair of relays. The

inverters' output currents are measured by LEM HX05-P transducers and the voltages are measured with LV25-P sensors. The control for each inverter developed in the Simulink simulations is compiled on a dSPACE CP1104 real-time controller, operating at a sample frequency of 7 kHz. Fig 18 shows the overall experimental set-up.

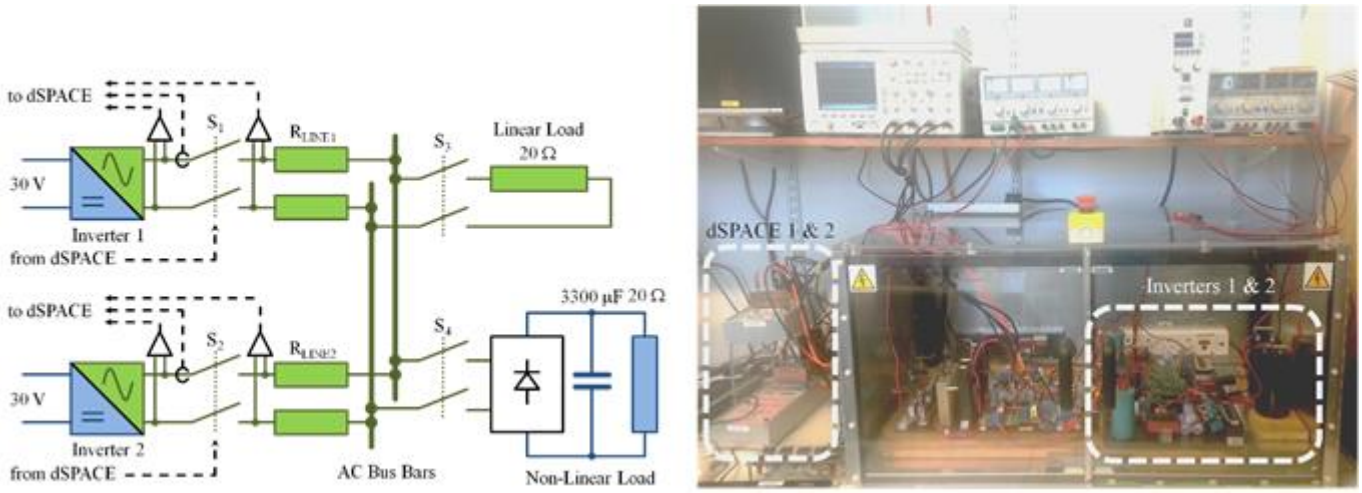

(a) **(b)**

Fig. 18. Experimental facility set-up (a) schematic and (b) hardware.

5. EXPERIMENTAL RESULTS

5.1. Reference Waveform Tracking and THD Measurements

The first experiment is to look at the reference waveform tracking performance for a single inverter. Inverter 1 in Fig. 18 is used with the diode rectified 20 Ω load. An FFT is also performed on the measured output voltage, to assess the low-order line-frequency harmonics, from the 1st to 15th harmonic. This experiment is carried out without and with the 3rd, 5th and 7th harmonic compensation loops. The results are shown in Fig 19. When the harmonic compensation is not used there is significant deviation between the reference waveform and output voltage, with a THD of 9.53%. When harmonic compensation is applied, the output voltage follows the reference waveform much closer, with 3rd, 5th and 7th harmonics suppressed to less than 0.01 V and an output voltage THD of 1.45%.

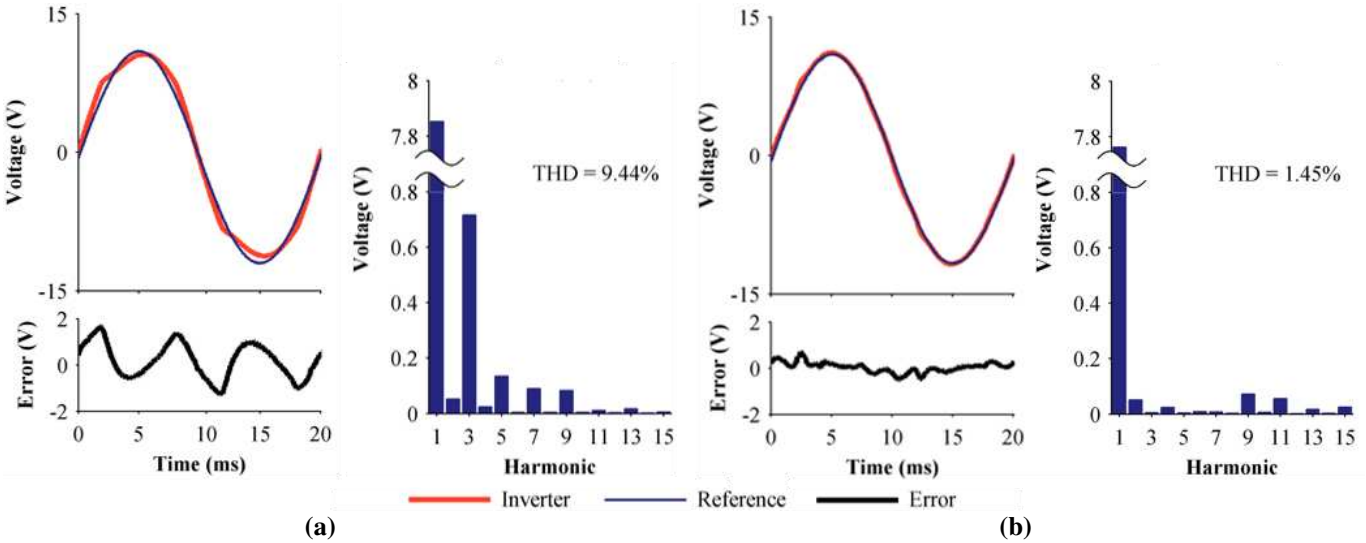

Fig. 19. Output voltage waveform in comparison with reference, tracking error between the two and output voltage THD when feeding a diode rectified load (a) without harmonic compensation and (b) with harmonic compensation

It is difficult to directly compare this method of harmonic compensation with others in the literature, as there is no standardised non-linear load to compare the performance against. However, comparing the output voltage THDs for alternative schemes such as those in [10], [11] and [17], which all have similar levels of output current distortion, with the experimental results presented here show that the THD reduction and the final output THD of less than 1.5% are very similar.

5.2. Synchronisation

The synchronisation performance of the inverters using the PLL and connection technique described in Section 2.6 is tested on the experimental set-up with equal power lines and no load connected, and shown in Fig. 20 (a). The synchronisation process is initiated at 52 ms, and within six line cycles the inverters are synchronised and ready to be connected together. When the inverters are connected, as in Fig. 20 (b) where inverter 1 is feeding a non-linear load initially, the connection is smooth, with the controller able to stabilise the output within two line cycles.

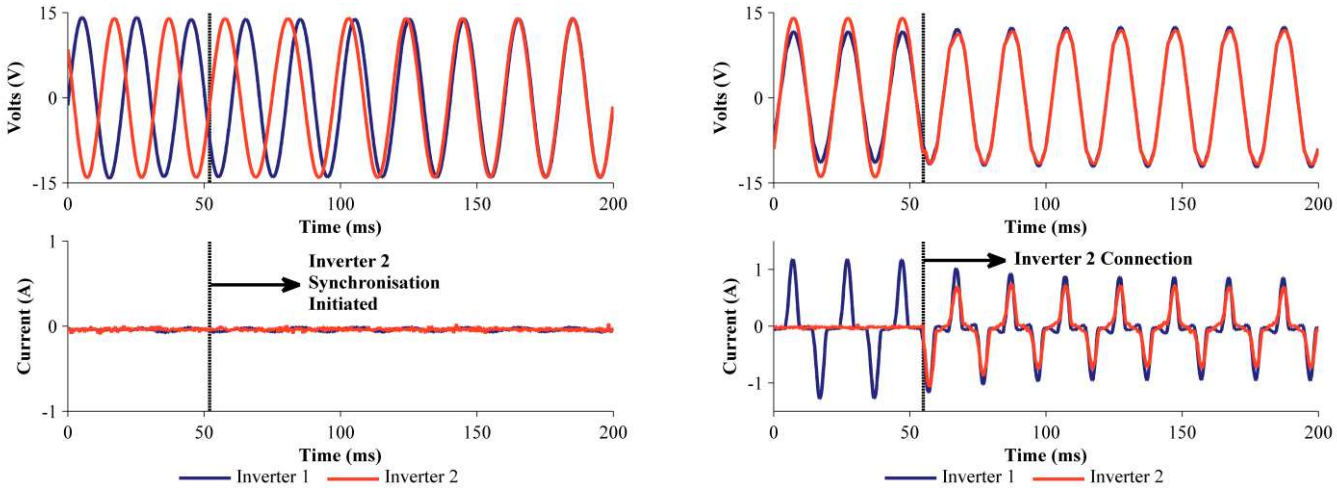

Fig. 20. (a) Synchronisation of inverter 2 with inverter 1. (b) Connection of two inverters feeding a non-linear load.

5.3. Power Sharing

With a view to examining the power sharing performance of the inverters when connected onto the AC bus bar, two scenarios are used; firstly with equal line impedances between each inverter the bus bar of 1 Ω and the secondly unequal line impedances with Z_{LINE1} = 1 Ω and Z_{LINE2} = 0.5 Ω. The power sharing experiments are run in steady state, with the inverters already synchronized and connected to a linear load, the steady-state voltage and current waveforms are shown in Fig. 21.

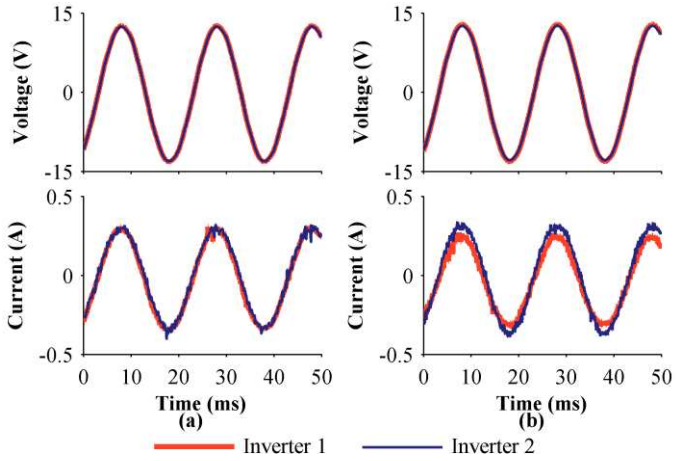

Fig. 21. Power sharing with (a) equal ($Z_{LINE1} = Z_{LINE2}$) and (b) unequal ($Z_{LINE1} = 2 \times Z_{LINE2}$) line impedances between the two inverters and the load

As can be seen from Fig. 21. (a), both inverters share the loads equally; therefore the circulating current between the two inverters is minimal. In Fig. 21 (b) the inverters now no longer equally share the load,

even though they have the same power output potential. Inverter 2 takes a larger share of the current at a ratio of 0.9:1, which matches the simulation in Section IV.

The available turbine power also affects the power sharing, through the normalized turbine output power ratio γ, which alters the droop curves and virtual impedance as shown in (6) – (8) in Section 2.1. With the two inverters synchronized and feeding the 20 Ω load with equal line impedances, the power rating ratio between inverters 1 and 2 is changed from 1:1 to 1:0.43 over a period of 5 seconds. This simulates a change in head at the turbine from 3.5 m to 2 m. The change in γ increases both the droop coefficients and the virtual resistance within the controller of inverter 2, altering the power sharing ratio between the two inverters. The output voltage and current waveforms for this are shown in Fig. 22 which shows that initially the load is being shared equally between the two inverters. When the power rating ratio changes from 1:1 to 1:0.43, the power sharing ratio between the two inverters reduces to 1:0.49. The discrepancy between these two ratios is due to a larger output current through inverter 2, which reduces the output voltage further through the virtual resistance.

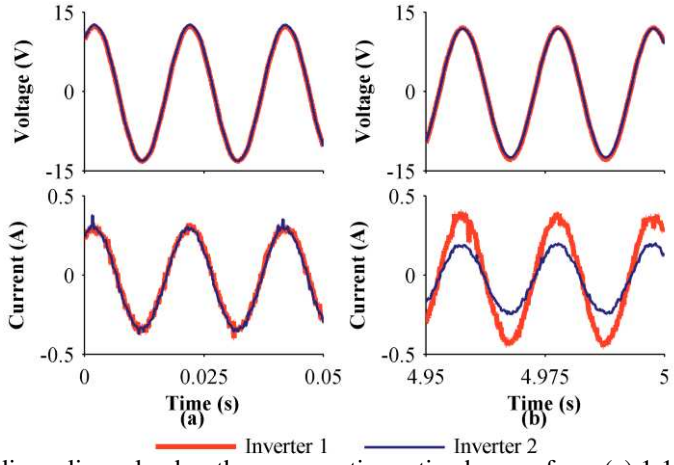

Fig. 22. Feeding a linear load as the power rating ratio changes from (a) 1:1 to (b) 1:0.43.

6. CONCLUSION

This paper has proposed a controller for parallel single-phase inverters in a pico-hydro off-grid network. The controller uses adaptations of known droop control techniques to achieve head-dependent voltage and frequency regulation without communication, and contains synchronous reference frame controllers for the fundamental voltage and current, and the voltage harmonics. The analytical model of the controller is presented showing the influence of design parameters on its performance. Simulation and experimentation

demonstrate the effectiveness of the proposed methodology. The introduction of a synchronous reference frame harmonic controller reduces the output voltage THD from 9.53% to 1.45%. The controller is also shown to successfully form an off‑grid network, as well as synchronise to and support an already formed network. When two inverters with equal input power are connected in parallel and the line impedances to the load are identical, the units are able to equally share the load. If the line impedances are different, then the power sharing ratio is no longer equal, reducing to 0.9:1 when the line impedances are at a ratio of 2:1. When there is a difference in power rating between units, the units are able to share the load in proportion to their respective ratings, for example, experiments showed that for a normalized turbine output power ratio of 1:0.43, the power sharing ratio was 1:0.49. The simulations and experiments show that the controller will be able to connect together a number of geographically-distant sources using only local measurements to control the power output to form an off-grid network. The computational overhead for the control algorithm is relatively high, requiring a fast processor and high sample frequency to operate the system.

When the controller is implemented in a system, such as that illustrated in Fig. 1 with multiple sites at varying heads using the same generation unit, there will be multiple generation and load nodes. All of these nodes have the potential to vary, therefore matching supply and demand is a challenge. For a well-designed pico-hydro system, the flow rate will be nearly constant, with changes happening over days and weeks, therefore the supply can be considered reasonably constant. Therefore, the demand management of the system is critical, requiring an in depth analysis of potential technical or social managerial solutions.

Further work in this project will include developing the complete power-electronic interface and carrying out a system simulation, experimental testing with a 1 kW-scale variable flow turbine, and improving the controller to reduce computational burden, as well as analysing the dynamic performance of the controller in an off-grid network with multiple supply and load nodes.

APPENDIX

The symbols used in (14)-(16) are listed below:

$$G_{1v} = k_{pv} + \frac{k_{iv}s}{s^2 + {\omega_{inv}}^2} \qquad G_{1i} = k_{pi} + \frac{k_{ii}s}{s^2 + {\omega_{inv}}^2}$$

$$G_{2v} = \frac{k_{iv}\omega_{inv}}{s^2 + {\omega_{inv}}^2} \qquad G_{2i} = \frac{k_{ii}\omega_{inv}}{s^2 + {\omega_{inv}}^2}$$

$$G_3 = \frac{CZ_{LD}s + 1}{LCZ_{LD}s^2 + (R_L CZ_{LD} + L)s + (R_L + Z_{LD})} \qquad G_4 = \frac{G_3 G_{1i}}{1 + G_3 G_{1i} G_\alpha - G_3 G_{2i} G_\beta}$$

$$G_5 = -\frac{G_3 G_{2i}}{1 + G_3 G_{1i} G_\alpha - G_3 G_{2i} G_\beta} \qquad G_6 = \frac{Z_{LD}}{CZ_{LD}s + 1}$$

$$G_7 = G_{1v} G_\alpha - G_{2v} G_\beta \qquad G_8 = G_{2v} G_\alpha + G_{1v} G_\beta$$

$$G_\alpha = \frac{k_\alpha s - k_\beta \omega_{inv}}{s^2 + k_\alpha s + \left(-k_\beta \omega_{inv} + {\omega_{inv}}^2\right)} \qquad G_\beta = \frac{k_\beta s + k_\alpha \omega_{inv}}{s^2 + k_\alpha s + \left(-k_\beta \omega_{inv} + {\omega_{inv}}^2\right)}$$

$$G_{1v,h} = k_{pvh} + \frac{k_{ivh}s}{s^2 + {\omega_{inv,h}}^2} \qquad G_{2v,h} = \frac{k_{ivh}\omega_{inv,h}}{s^2 + {\omega_{inv,h}}^2}$$

$$G_{3,h} = \frac{Z_{LD}}{LCZ_{LD}s^2 + (R_L CZ_{LD} + L)s + (R_L + Z_{LD})}$$

$$G_{\alpha,h} = \frac{k_{\alpha h}s - k_{\beta h}\omega_{inv,h}}{s^2 + k_{\alpha h}s + \left(-k_\beta \omega_{inv,h} + {\omega_{inv,h}}^2\right)} \qquad G_{\beta,h} = \frac{k_{\beta h}s + k_{\alpha h}\omega_{inv,h}}{s^2 + k_{\alpha h}s + \left(-k_\beta \omega_{inv,h} + {\omega_{inv,h}}^2\right)}$$

where k_{pi}, k_{ii} k_{pv}, k_{iv} are the proportional and integral gains of the current and voltage fundamental component controllers, respectively; h is the harmonic order, k_{pvh} and k_{ivh} are the proportional and integral controller gains for the h-th voltage harmonic, and $\omega_{inv,h}$ is the harmonic frequency; k_α and k_β are the gains for the SOGI-based filter, ω_{inv} is the line frequency, L and C are the output filter inductance and capacitance, R_L is the output filter inductor's parasitic resistance, and Z_{LD} is the load impedance.

REFERENCES

[1] A. A. Williams and R. Simpson, "Pico hydro - Reducing technical risks for rural electrification," Renewable Energy, vol. 34, pp. 1985-1991, 2009.

[2] N. P. A. Smith, "Induction generators for stand-alone micro-hydro systems," in *Proc. Int. Conf. Power Electron, Drives and Energy Syst. for Ind. Growth*, New Delhi, 1996, pp. 669-673.

[3] P. Maher, N. P. A. Smith and A. A. Williams, "Assessment of pico hydro as an option for off-grid electrification in Kenya," Renewable Energy, vol. 28, no. 9, pp. 1357-1369, July 2003.

[4] B. Shakya, "Piloting A Minigrid in Baglung District," Alternative Energy Promotion Centre, Renewable Energy for Rural Livelihood Programme, Lalitpur, 2012.

[5] A. Engler, "Applicability of Droops in Low Voltage Grids," Int. J. of Distributed Energy Resources, vol. 1, no. 1, pp. 1-5, 2005.

[6] J. M. Guerrero et al, "Decentralized Control for Parallel Operation of Distributed Generation Inverters Using Resistive Output Impedance," *IEEE Trans. Ind. Electron.*, vol. 54, pp. 994-1004, 2007.

[7] J. M. Guerrero et al, "Steady-state invariant frequency and amplitude droop control using adaptive output impedance for parallel-connected UPS inverters," in *Proc. IEEE Appl. Power Electron. Conf.*, Austin, 2005, pp. 560-566.

[8] Q. C. Zhong, "Robust droop controller for accurate proportional load sharing among inverters operated in parallel," *IEEE Trans. Ind. Electron.*, vol. 60, pp. 1281-1290, 2013.

[9] K. de Brabandere et al, "A Voltage and Frequency Droop Control Method for Parallel Inverters," *IEEE Trans. Power Electron.*, vol. 22, pp. 1107-1115, 2007.

[10] M. Monfared et al, "Analysis, Design, and Experimental Verification of A Synchronous Reference Frame Voltage Control for Single-Phase Inverters," *IEEE Trans. Ind. Electron.*, vol. 61, pp. 258-269, 2014.

[11] A. Micallef et al, “Reactive power sharing and voltage harmonic distortion compensation of droop controlled single phase islanded microgrids”, *IEEE Trans. Smart Grid*, vol. 5, pp. 1149-1158, 2014.

[12] M. N. Marwali, J. Jung, A. Keyhani, “Control of Distributed Generation Systems – Part II: Load Sharing Control”, *IEEE Trans. Power Electron.*, vol. 19, pp. 1551-1531, 2004.

[13] Q. C. Zhong and G. Weiss, “Synchronverters: Inverters That Mimic Synchronous Generators”, *IEEE Trans. Ind. Electron.*, vol. 58, pp. 1259-1267, 2011.

[14] H. P. Beck and R. Hesse, “Virtual synchronous machine”, in *Proc. 9th Int. Conf. Elect. Power Quality and Utilisation*, Barcelona, 2007, pp. 1-6.

[15] Q. C. Zhong and T. Hornik, Control of Power Inverters in Renewable Energy and Smart Grid Integration, Chichester: John Wiley & Sons Ltd, 2013, Chap. 2.

[16] S. J. Chiang and J. M. Chang “Parallel operation of series-connected PWM voltage regulators without control interconnection”, *IEE Proc. Electric Power Appl.*, vol. 148, pp. 141-147, 2001.

[17] Q. C. Zhong, “Harmonic Droop Controller to Reduce the Voltage Harmonics of Inverters,” *IEEE Trans. Ind. Electron.*, vol. 60, pp. 936-945, 2013.

[18] M. Ciobotaru et al, “A New Single-Phase PLL Structure Based on Second Order Generalised Integrator,” in *Proc. IEEE Power Electron. Specialists Conf.*, Jeju, 2006, pp. 1-6.

[19] Q. C. Zhong and Y. Zeng, “Parallel Operation of Inverters with Different Types of Output Impedance”, in *Proc. IEEE Ind. Electon. Conf.*, Vienna, 2013, pp. 1398-1403.

[20] S. J. Williamson, B. H. Stark and J. D. Booker, “Performance of a low-head pico-hydro Turgo turbine,” Applied Energy, vol. 102, pp. 1114-1126, 2013.

[21] J. L. Márqueza, M. G. Molinab, and J. M. Pacasc, “Dynamic modeling, simulation and control design of an advanced micro-hydro power plant for distributed generation applications,” International Journal of Hydrogen Energy, vol. 35, pp. 5772–5777, 2010

[22] G. Muller and J. Senior, “Simplified theory of Archimedean screws,” Journal of Hydraulic Research, vol. 47, pp. 666–669, 2009.

[23] S. J. Williamson, B. H. Stark and J. D. Booker, “Low head pico hydro turbine selection using a multi-criteria analysis,” Renewable Energy, vol. 61, pp 43-50, 2014.

[24] A. Roshan et al, “A D-Q Frame Controller for a Full-Bridge Single Phase Inverter Used in Small Distributed Power Generation Systems,” in *Proc. IEEE Appl. Power Electron. Conf.*, Anaheim, 2007, pp. 641-647.

[25] B. Burger and A. Engler, “Fast Signal Conditioning in Single Phase Systems,” in *Proc. European Power Electron. and Drives Conf.*, Graz, 2001.

[26] K. de Brabandere et al, “Design and Operation of a Phase-Locked Loop with Kalman Estimator-Based Filter for Single-Phase Applications,” in *Proc. IEEE Conf. on Ind. Electron.*, Paris, 2006, pp. 525-530.

[27] C. A. Busada, S. Gómez Jorge, A. E. Leon, and J. A. Solsona, “Current Controller Based on Reduced Order Generalized Integrators for Distributed Generation Systems,” *IEEE Trans. Ind. Electron.,* vol. 59, pp. 2898-2909, 2012.

[28] M. Liserre , R. Teodorescu and F. Blaabjerg "Multiple harmonics control for three-phase grid converter systems with the use of PI-RES current controller in a rotating frame", *IEEE Trans. Power Electron.*, vol. 21, pp.836 -841 2006.

[29] C. Lascu , L. Asiminoaei , I. Boldea and F. Blaabjerg "Frequency response analysis of current controllers for selective harmonic compensation in active power filters", *IEEE Trans. Ind. Electron.*, vol. 56, pp.337 -347, 2009.

[30] R. Zhang et al, “A grid simulator with control of single-phase power converters in D-Q rotating frame,” in *Proc IEEE Annu. Power Electron. Specialists Conf.*, Cairns, 2002, pp. 1431-1436.

[31] M. Karimi-Ghartemani, “Universal Integrated Synchronization and Control for Single Phase DC/AC Converters”, *IEEE Trans. Power Electron.*, in press, DOI 10.1109/TPEL.2014.2304459

[32] B. Bahrani, et al, "A Multivariable Design Methodology for Voltage Control of a Single-DG-Unit Microgrid", *IEEE Trans. Ind. Informat.*, vol. 9, pp. 589-599, 2013.

[33] B. Bahrani , A. Rufer , S. Kenzelmann and L. Lopes "Vector control of single-phase voltage source converters based on fictive axis emulation", *IEEE Trans. Ind. Appl.*, vol. 47, pp.831-840, 2011.

[34] D. N. Zmood and D. G. Holmes, “Stationary Frame Current Regulation of PWM Inverters With Zero Steady-State Error,” *IEEE Trans. Power Electron.*, vol. 18, pp. 814-822, 2003.

[35] P. Mattavelli, “A closed-loop selective harmonic compensation for active filters”, *IEEE Trans. Ind. Appl.*, vol. 37, pp. 81-89, 2001.

[36] Y. Xiaoming, W. Merk, H. Stemmler, J. Allmeling, “Stationary-frame generalized integrators for current control of active power filters with zero steady-state error for current harmonics of concern under unbalanced and distorted operating conditions”, *IEEE Trans. Ind. Appl.*, vol.38, pp. 523-532, 2002.

[37] S. Golestan, M. Monfared, F. D. Freijedo, J. M. Guerrero, "Dynamics Assessment of Advanced Single-Phase PLL Structures,” *IEEE Trans. Ind. Electron.*, vol. 60, pp. 2167-2177, 2013.

[38] S. Golestan, M. Monfared, F. D. Freijedo, J. M. Guerrero, "Advantages and Challenges of a Type-3 PLL," *IEEE Trans. Power Electron.,* vol. 28, pp. 4985-4997, 2013.

[39] H. Geng; J. Sun; S. Xiao; G. Yang "Modeling and Implementation of an All Digital Phase-Locked-Loop for Grid-Voltage Phase Detection", *IEEE Trans. Ind. Informat.*, vol. 9 pp. 772-780, 2013.

[40] P. Rodriguez , A. Luna , I. Candela , R. Mujal , R. Teodorescu and F. Blaabjerg "Multiresonant frequency-locked loop for grid synchronization of power converters under distorted grid conditions", *IEEE Trans. Ind. Electron.*, vol. 58, pp. 127-138, 2011.

[41] J. M. Guerrero, J. C. Vasquez, J. Matas, L. G. de Vicuna, M. Castilla, "Hierarchical Control of Droop-Controlled AC and DC Microgrids—A General Approach Toward Standardization", *IEEE Trans. Ind. Electron.,* vol. 58, pp. 158-172, 2011.

[42] M. Salcone and J. Bond, "Selecting film bus link capacitors for high performance inverter applications," in *Proc. Int. Electric Machines and Drives Conf.*, Miami, 2009, pp. 1692–1699